Crystallographic disorder and electron-phonon coupling in $Fe_{1-x}Co_xSi$ single crystals: Raman spectroscopy study

A.-M. Racu,* D. Menzel, and J. Schoenes
Institut für Physik der Kondensierten Materie, Technische Universität Braunschweig, Mendelssohnstrasse 3, D-38106 Braunschweig, Germany

K. Doll
Max-Planck-Institut für Festkörperforschung, Heisenbergstrasse 1, D-70569 Stuttgart, Germany
(Received 16 March 2007; revised manuscript received 29 May 2007; published 6 September 2007)

A comprehensive concentration and temperature dependent Raman spectroscopy study of $Fe_{1-x}Co_xSi$ with x between 0 and 1 is presented. All the nine Raman active modes predicted by the factor group analysis are observed in our experiments. A detailed analysis of the symmetry of the Raman lines and a comparison with IR spectroscopy helps assign the observed peaks to modes with A, E, or T symmetry. Local density approximation calculations of the phonon frequencies in FeSi and CoSi match very well the experiments. The concentration dependence of the Raman linewidth with a maximum around $x=0.5$ points to crystallographic disorder in the substituted systems. For the semiconducting compounds ($x \lesssim 0.1$), the temperature dependence of the Raman linewidth reveals strong electron-phonon interactions. The fit of this temperature dependence gives an activation energy of 30 meV in accordance with the semiconducting gap of FeSi.

DOI: 10.1103/PhysRevB.76.115103 PACS number(s): 71.20.Be, 63.20.−e

I. INTRODUCTION

The physical properties of FeSi have been interpreted using either itinerant or localized models for the electronic states. There is not yet an agreement which of these models is best suitable. Optical reflectivity,[1–3] tunneling spectroscopy,[4,5] transport measurements,[6] and photoemission[7] claimed the existence of an energy gap of the order of 60 meV at low temperature. This small gap closes on increasing the temperature to 200 K, a value less than one-third of the activation energy,[1] which has been taken as indication that FeSi is a hybridization-gap semiconductor or Kondo insulator. Nyhus *et al.*[8] observed an isosbestic point in the temperature dependence of the electronic Raman signal and interpreted it also in a strong correlation model. On the other hand, band structure calculations[9] and magnetic measurements for the mixed compounds $Fe_{1-x}Co_xSi$ under ambient[10] or high pressure[11] support an itinerant picture. Also, Zur *et al.*[12] did not find any sign of Kondo resonance in high-resolution photoemission experiments of FeSi and concluded that the one particle band structure calculation describes this system better than the Kondo model. In addition, a deconvolution of the spectra near the Fermi energy points to a gap of $\approx$30 meV, i.e., substantially smaller than assumed before.

In this paper, we present a comprehensive analysis of the Raman active phonons for FeSi, CoSi, and for $Fe_{1-x}Co_xSi$ with x between 0 and 1. It is interesting to study all concentrations because drastic changes occur in the physical properties of these materials with increasing Co content: the gap disappears and the magnetic properties change from a paramagnetic semiconductor (FeSi) to ferromagnetic ordering for almost all Co compositions x and, finally, to a diamagnetic metal (CoSi). We monitor this semiconductor to metal phase transition with Raman spectroscopy and analyze the typical changes which occur when the transition metal is substituted.

II. THEORY

A. Crystal symmetry

FeSi, CoSi, and the mixed concentration compounds $Fe_{1-x}Co_xSi$ crystallize in the so called $B20$ structure in the space group $P2_13$, with 4 f.u. per unit cell. The Fe (Co) and Si atoms occupy the Wyckoff positions $4a$ with the coordinates (u,u,u), $(1/2+u,1/2-u,-u)$, $(-u,1/2+u,1/2-u)$, and $(1/2-u,-u,1/2+u)$. A schematic picture of this structure is presented in Fig. 1.

B. Factor group analysis

For a correct interpretation of the experimental data, a prior calculation of the number and symmetry of the Raman and infrared (IR) active modes is very useful. The factor group analysis (FGA) offers a mathematical support for this calculation using the symmetry of the crystal and the site occupation as input data. Yet, the FGA can only predict the maximum number of Raman and IR active modes and their symmetry. No information about the position and intensity of the modes is available from the FGA. Moreover, the FGA cannot differentiate between the vibrations of different atoms

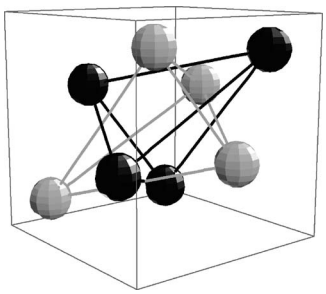

FIG. 1. Unit cell of the $B20$ structure. The gray circles represent Fe (Co) atoms and the black circles represent Si atoms.

TABLE I. Results of the FGA for the *B*20-type structure.

Material	Raman active modes	IR active modes
FeSi	$2A+2E+5T$	$5T$

which occupy the same Wyckoff position (in our case, the Fe and Si atoms are both on 4*a* symmetry site). An approximate mode assignment is possible if one remembers that the frequency of a Raman line is inversely proportional to the square root of the weight of the vibrating atoms. In our case, we expect that the Fe (Co) modes have lower frequency than the Si modes.

A summary of the results of the phonon calculation for the *B*20-type structure is presented in Table I.

There are nine optical active modes all together ($2A+2E+5T$), all are Raman active and the $5T$ modes are also IR active. *A* are nondegenerate species, *E* are doubly degenerate modes, and *T* are triply degenerate modes.

We can determine the angular dependence of the Raman intensity for the Raman active modes listed in Table I using Eq. (1)

$$I_k \sim \left| \sum_{i,j=1,2,3} e_i^l R_{ij}^k e_j^s \right|^2. \quad (1)$$

The intensity I_k of a Raman line depends on the polarizations e_i^l and e_j^s of the incident and scattered light, respectively, and on the Raman tensor element R_{ij}.[13] This helps in the interpretation of the measured spectra and the correct assignment of the phonons to the symmetry species. The Raman tensors for the three symmetry types are listed below:

$$A: \begin{pmatrix} a & 0 & 0 \\ 0 & a & 0 \\ 0 & 0 & a \end{pmatrix},$$

$$E: \begin{pmatrix} b+c\sqrt{3} & 0 & 0 \\ 0 & b-c\sqrt{3} & 0 \\ 0 & 0 & -2b \end{pmatrix}, \begin{pmatrix} c-b\sqrt{3} & 0 & 0 \\ 0 & c+b\sqrt{3} & 0 \\ 0 & 0 & -2c \end{pmatrix},$$

$$T: \begin{pmatrix} 0 & 0 & 0 \\ 0 & 0 & d \\ 0 & d & 0 \end{pmatrix}, \begin{pmatrix} 0 & 0 & d \\ 0 & 0 & 0 \\ d & 0 & 0 \end{pmatrix}, \begin{pmatrix} 0 & d & 0 \\ d & 0 & 0 \\ 0 & 0 & 0 \end{pmatrix}.$$

We observe that the Raman tensor for the *A* modes has a totally symmetric form. Applying Eq. (1), we can deduce a selection rule which is independent of the sample orientation: the *A* modes are visible in the spectra only when the incident and the scattered light polarizations are parallel. For the *E* and *T* symmetry modes, it is not easy to make a prediction when the orientation of the sample is not known. However, these modes will generally have nonzero components in parallel and perpendicular polarization configurations and complicated angular dependent patterns.

Figure 2 presents the phonon eigenvectors for the *A*, *E*, and *T* symmetry species. The unit cell was rotated in order to observe clearly which atoms vibrate against each other.

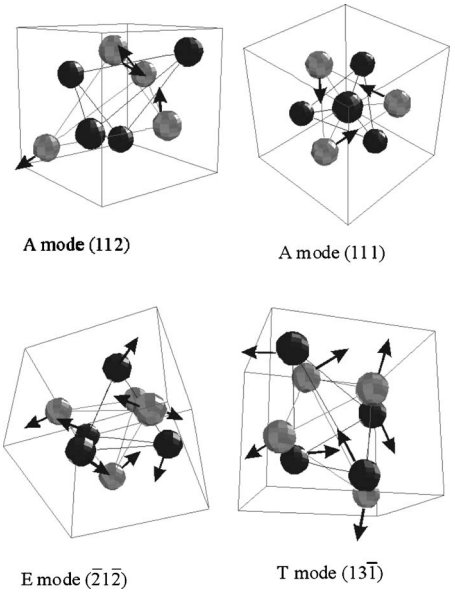

FIG. 2. The eigenvectors of the vibration modes for *A*, *E*, and *T* symmetry species. Gray and black circles represent transition-metal and Si atoms, respectively. The unit cell was rotated near the directions given in the brackets for an optimal image of the vibrations.

C. Local density approximation calculation of the phonon frequencies

Density functional calculations were performed for the systems FeSi and CoSi to compute the vibrational frequencies from first principles. The calculations were performed with the code CRYSTAL,[14] which is based on a local Gaussian basis set. As had been shown previously,[12,15,16] the ground state properties of the system FeSi are reasonably well described within the framework of the local density approximation (LDA). The Gaussian basis set for FeSi was the one described in Ref. 16. The CoSi exponents were reoptimized using a fcc structure. The Co basis set from Ref. 17 was modified in the following way: two *sp* shells (exponents 0.61 and 0.16) were used (instead of the single exponent 0.6031), and the outermost *d* exponent was reoptimized (0.26 instead of 0.3011). The outermost Si exponents were reoptimized, and values of 0.49 (FeSi: 0.45) 0.18 (as in FeSi) for the *sp* shells and 0.57 (FeSi: 0.53) for the *d* shell were obtained. A $\vec{k}$-point sampling net of the size $8\times8\times8$ was used, and in the case of CoSi, a smearing temperature of 0.01 E_h ($\sim$0.27 eV) was used. The frequencies were computed by using a combined analytical first[18,19] and numerical second derivative,[20] and the IR intensities were computed based on the modern theory of polarization[21–23] using localized Wannier functions.[24]

The step size to compute the frequencies was enlarged to 0.01 Å (compared to the default value of 0.001 Å) which was found to lead to a significantly higher stability of especially the computed infrared intensities.

III. EXPERIMENT

High quality $Fe_{1-x}Co_xSi$ single crystals have been grown by the triarc Czochralski method using 99.98% Fe, 99.9

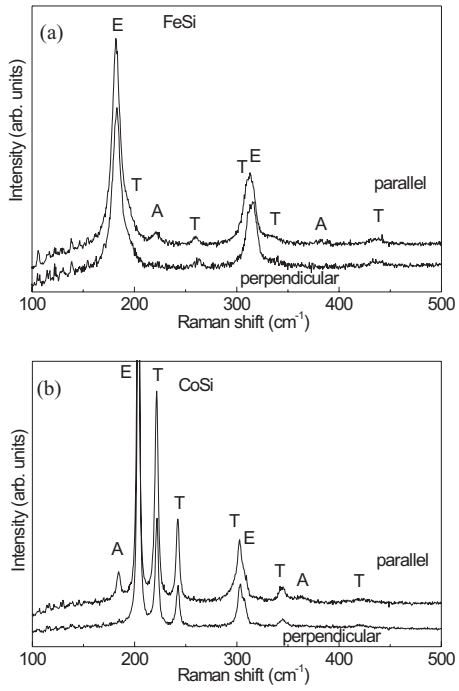

FIG. 3. Room temperature polarization resolved Raman spectra of (a) FeSi and (b) CoSi.

+% Co, and high purity Si (ρ_n=300 Ω cm, ρ_p=3000 Ω cm). Each crystal has been cut into several disks with a typical diameter of 5 mm. Some FeSi crystals cut from the same batch have been oriented with x rays and low energy electron diffraction for photoemission experiments[12] and showed good crystallinity. From susceptibility measurements of pure FeSi at low temperature, a concentration of magnetic impurities of 0.17% was derived. The crystals used in this experiment have not been oriented, which does not affect the results of the Raman investigations.

Raman spectra have been recorded using a commercial micro-Raman spectrometer (Jobin Yvon LabRam HR), operated with a notch filter and a grating monochromator. The excitation radiation is the 532 nm wavelength line of a diode-pumped Nd-doped yttrium aluminum garnet laser of 150 mW. The light beam is focused on an area of a few μm^2, depending on the choice of the microscope objective. The resolution is about 2.3 cm^{-1}. For polarization resolved measurements, the direction of the laser polarization was rotated with a $\lambda/2$ plate, while the direction of the analyzer in front of the monochromator was kept constant. The temperature dependent measurements were performed using a KONTI cryostat-type Micro between 4 and 320 K.

IV. RESULTS AND DISCUSSION

Figure 3 displays the Raman spectra of FeSi and CoSi for two different polarization configurations: parallel and perpendicular. According to the selection rules discussed above, it is possible to assign the A symmetry modes. In order to identify the E and T symmetry modes, we compare the Raman results with the IR measurements.[27] The T modes are visible in both Raman and IR, while the E modes are only Raman active.

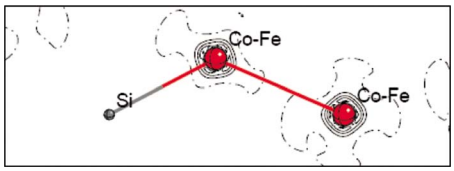

FIG. 4. (Color online) Charge density difference CoSi-FeSi, in a plane made of a Co atom, a nearest neighbor Si atom, and another nearest neighbor Co atom. Zero difference is indicated by a dashed line, and the full lines have a distance of 0.2 $\frac{|e|}{a_0^3}$ with the Bohr radius a_0.

In the calculations, first, a geometry optimization was performed for CoSi, and an equilibrium lattice constant of 4.37 Å was obtained, with internal parameters of u_{Si}=0.843 and u_{Co}=0.145 and a bulk modulus of B=255 GPa. The geometrical values are in excellent agreement with recent LDA results.[25] The lattice constant is slightly shorter compared to experiment [~4.44 Å (Ref. 26)], which is usually observed in LDA calculations. Similarly, the computed FeSi lattice constant of 4.38 Å is slightly shorter than the experimental lattice constant of 4.49 Å.[26] The Mulliken population results in a charge of −0.48 $|e|$ for Co, and thus +0.48 $|e|$ for Si, which is similar to FeSi (Ref. 16) where charges of −0.64 $|e|$ for Fe and thus 0.64 $|e|$ for Si were computed. Compared to FeSi, the additional electron thus essentially resides at the Co site. This is also clearly shown in the charge density difference plot in Fig. 4. In this figure, the charge density of FeSi was subtracted from that of CoSi, with both systems having the geometrical parameters as in the CoSi lattice, to make a comparison easier.

The band structure is displayed in Fig. 5. Compared to FeSi,[15] the bands are similar and the main difference is that the Fermi level has been shifted due to the additional electron so that the system has become metallic.

In Fig. 6, the Raman experiments are compared with the calculated mode frequencies. Notice a perfect match of the succession of the A, E, and T Raman modes, while the ab-

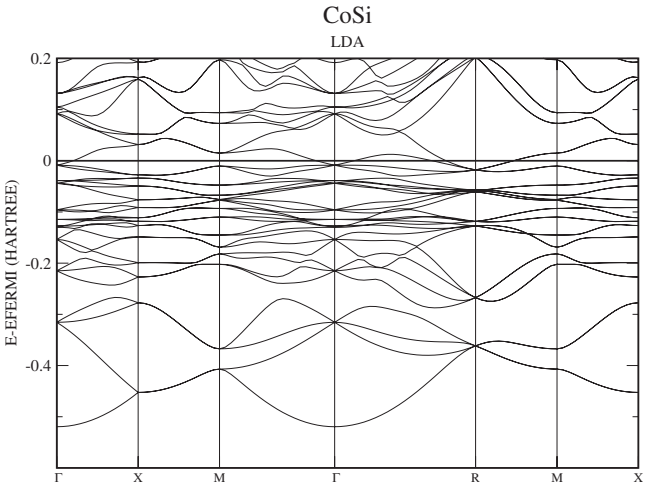

FIG. 5. LDA band structure of CoSi.

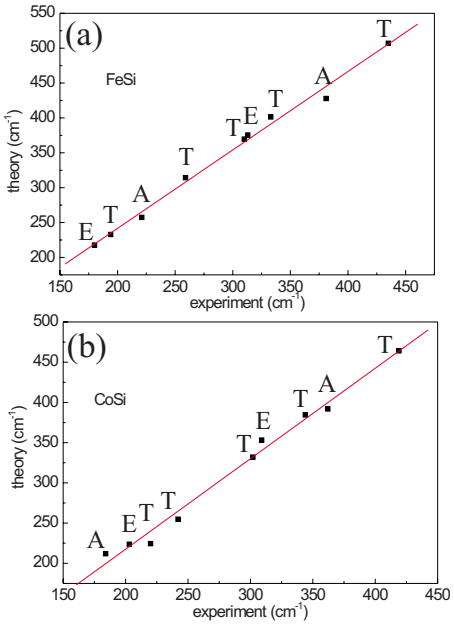

FIG. 6. (Color online) Comparison between the measured (abscissa) and calculated (ordinate) phonon frequencies in (a) FeSi and (b) CoSi. The lines are linear fits with a slope of 1.12 for both systems.

solute values of the frequencies are slightly different. The theory vs experiment curves were fitted by linear functions. The slope of the line is 1.12 for both systems. This small deviation from unity is consistent with the computed structural data: the LDA potential is too attractive, and thus the lattice constant computed at the LDA level is too short. Therefore, also the computed bulk moduli and vibrational frequencies are too large.

While in FeSi the factor of 1.12 is constant for all the phonons, we see that in CoSi there are some modes that deviate somewhat more from the straight line. One needs to consider that Co has one more electron than Fe which additionally affects the potential. The theory reproduces nicely the striking shift in the phonon frequency of the low *A* mode from 221 cm^{-1} in FeSi to 184 cm^{-1} in CoSi (see also Tables II and III). At the same time, the *E* mode at 180 cm^{-1} and the *T* mode at 194 cm^{-1} harden substantially to 204 and 221 cm^{-1}, respectively. From graphical animations of the computed modes, it becomes obvious that the lower *A* mode is a pure vibration of the transition metal (see Fig. 2). Due to the presence of free electrons in CoSi, the lattice potential is screened and one generally would expect a softening of the Raman modes. On the other hand, the CoSi lattice constant is slightly shorter than the FeSi lattice constant, which could explain higher frequencies. Only a very small shift is due to the different atomic masses of Fe and Co, but the strong effect observed is a consequence of the semiconductor to metal transition with increasing x and the change of the lattice constant.

Tables II and III present the measured and calculated vibration frequencies of FeSi and CoSi, respectively. Computed IR intensities are included in the table, whereas Raman intensities cannot yet be computed. We were able to measure and identify all the nine Raman active phonons predicted by the FGA (Table I). The Raman scattering measurements performed by Nyhus *et al.*[8] could not resolve the *A* mode at 381 cm^{-1}. In the IR ellipsometry measurements of Menzel *et al.*,[27] the *T* mode at 259 cm^{-1} is absent due to a negligible matrix element. Indeed, in the calculations it is found that the IR intensity of this mode is extremely small compared to the other infrared-active modes.

For CoSi, there are no Raman measurements available in the literature. The positions of the *T* symmetry modes determined in the present work match very well the IR modes measured by Menzel *et al.*[27] on the same sample, as shown in Table III.

We will now discuss the pseudobinary compounds $Fe_{1-x}Co_xSi$. These mixed concentration compounds have already been studied using different methods such as photoemission,[10,29] magnetic,[30] transport,[31] and IR measurements.[32] The experiments gave information on the closing of the gap and changes in the magnetic and transport properties. Our Raman measurements show dramatic changes corroborating the semiconductor to metal transition. Furthermore, we will show that there is a large electron-phonon coupling in the semiconducting samples with $x \lesssim 0.1$, while for higher Co concentrations, where the system is metallic, we found no sign of electron-phonon coupling.

Before discussing the evidence for electron-phonon coupling, it is important to know which role is played by the

TABLE II. Positions in cm^{-1} and computed IR intensities in km/mole (in brackets) of the Raman active modes in FeSi. The experimental values are obtained at room temperature.

	Raman (this work)	Raman (Ref. 8)	IR (Ref. 27)	Theory (this work)	
A	221	219		257	
A	381			428	
E	180	180		218	
E	313	315		376	
T	194	193	195	233	(2137)
T	259	260		314	(6)
T	310	311	320	370	(6505)
T	333	333	338	401	(1655)
T	435	436	447	507	(2141)

TABLE III. Positions in cm^{-1} of the Raman active modes in CoSi. The experimental values are obtained at room temperature.

	Raman (this work)	IR (Ref. 27)	Theory (this work)
A	184		212
A	362		392
E	203		225
E	309		353
T	220	224	224
T	242		255
T	302	306	332
T	344	347	384
T	419	424	464

crystallographic disorder in the Raman spectra of the mixed $Fe_{1-x}Co_xSi$ compounds. Figure 7 displays Raman spectra for samples with different Co concentrations x recorded at a temperature of 5 K. We observe a consequent broadening of the Raman lines (most obvious for the dominant *E* mode at about 180 cm^{-1}) as the Co concentration increases up to $x=0.5$ followed by a decrease of the linewidth between $x=0.5$ and $x=1$.

The linewidth of a Raman phonon contains, on one hand, information on the anharmonicity of the lattice potential. The anharmonic effect has been successfully described with perturbation theory. In this approach, the broadening of a Raman line is given by the decay of the optical phonon into two acoustic modes, which has been successfully described using Boltzmann functions.[33,34] Consequently, the effect is drastically reduced if the measurements are performed at low temperatures.

On the other hand, compositional disorder and poor crystallinity may affect the vibrational properties of mixed crystals in the form of a temperature independent linewidth broadening of phonon modes. In our experiments, Co is introduced in the FeSi matrix as an impurity and implicitly causes disorder. We can use the linewidth of the phonon at 5 K, Γ, as a disorder parameter. Figure 8 presents the dependence of this disorder parameter on the Co concentration x in the mixed crystals $Fe_{1-x}Co_xSi$. The largest linewidth is observed for the compound with $x=0.5$. This is not surprising since this composition has the highest substitutional disorder.

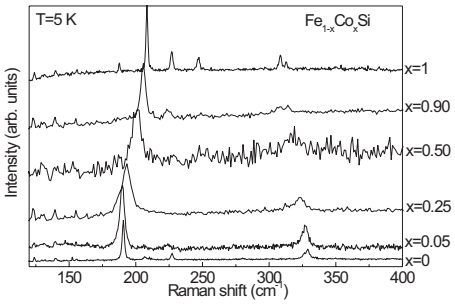

FIG. 7. Raman spectra of $Fe_{1-x}Co_xSi$ samples with different Co concentrations x at 5 K.

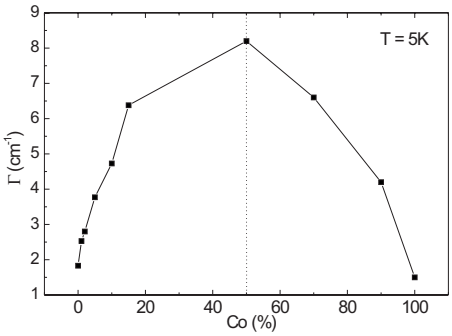

FIG. 8. The linewidth of the *E* mode (180 cm^{-1}) at 5 K as a function of the Co concentration x. The linewidth was determined using the perpendicular configuration in order to avoid the effect of the overlapping *A* and *E* modes for intermediate concentrations.

Moreover, the symmetric curve in Fig. 8 is a proof that the samples are free from other random impurities and are of a very good crystallinity.

We are now ready to discuss the effect of the electron-phonon coupling. To this goal, Fig. 9 shows the temperature dependence of the linewidth of the lowest *E* phonon at about 180 cm^{-1}. One clearly sees two different types of behavior. For the semiconducting samples, i.e., for $x \lesssim 0.1$, the linewidth increases strongly with increasing temperature and saturates above approximately 250 K. In contrast, the metallic samples, i.e., those with $x > 0.1$, display a much weaker temperature dependence of the linewidth. Additional measurements well above room temperature (not shown here) corroborate as well the saturation for the semiconducting samples as the slight increase for the metallic samples.

A strong broadening of the *E* line in FeSi has also been observed by Nyhus *et al.*[8] Other systems such as superconducting materials[35] or metal hydrides[36] also show an anomalous broadening of one Raman line with increasing temperature. Following the theory used by Axe and Shirane[37] for superconducting materials, the ratio Γ/ω_0 for a particular mode is a direct estimate of that phonon's contribution to the electron-phonon coupling parameter:

$$\Gamma/\omega_0 = \pi N(0)\hbar\omega_0\lambda. \quad (2)$$

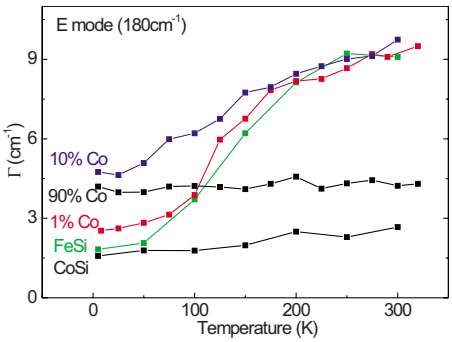

FIG. 9. (Color online) The linewidth of the *E* mode (180 cm^{-1}) as a function of temperature for several samples with different Co concentrations.

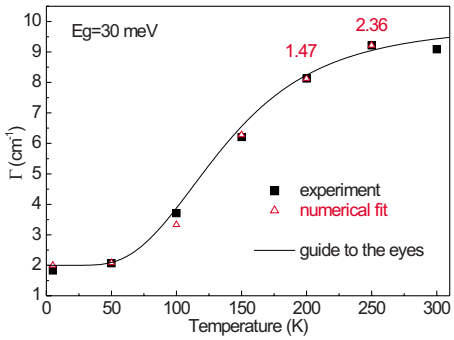

FIG. 10. (Color online) The linewidth of the E mode (180 cm^{-1}) of FeSi as a function of temperature (squares). The triangles represent the numerical integration of Eq. (3) using an activation energy of 30 meV. The m_n/m_p ratio is equal to 1 for $T<150$ K and increases to 1.47 and 2.36 for 200 and 250 K, respectively.

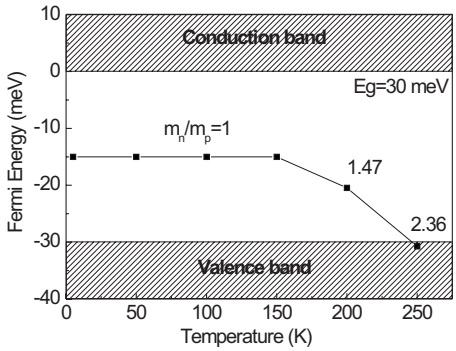

FIG. 11. Model of the temperature dependence of the Fermi energy in FeSi.

Here, $N(0)$ is the electronic density of states at the Fermi surface, ω_0 is the mode frequency, and λ is its contribution to the electron-phonon coupling parameter.

We have discussed above that structural disorder effects do not induce a temperature dependence of the linewidth. On the other hand, anharmonic effects, i.e., phonon-phonon interactions, are described by Boltzmann functions and do not saturate. Thirdly, electron-phonon interactions follow the temperature dependence of the electronic density of states at E_F. Therefore, we explain the peculiarities of the temperature dependence of the Raman linewidths as follows.

(i) For semiconducting FeSi and $Fe_{1-x}Co_xSi$ with $x \lesssim 0.1$, at low temperatures the band gap is open and there are no free electrons in the conduction band which could couple to the phonons. As the temperature rises, the excited electrons provide a mechanism for phonon decay. The concentration of excited electrons in the conduction band is given by[38]

$$n(T) = 2\left(\frac{m_n kT}{2\pi\hbar^2}\right)^{3/2} \frac{2}{\sqrt{\pi}} \int_0^\infty d\eta \frac{\eta^{1/2}}{1+\exp(\eta-\zeta)}, \qquad (3)$$

with $\eta=(E-E_C)/kT$ and $\zeta=(E_F-E_C)/kT$. E_C is the lower edge of the conduction band and E_F is the Fermi energy. The chemical potential E_F-E_C is a function of the temperature and the ratio m_n/m_p (m_n and m_p being the effective masses of the electrons and holes, respectively). FeSi is a narrow gap semiconductor, for which E_F-E_C is of the order of kT already at room temperature. Therefore, we cannot neglect the 1 in the denominator under the integral in Eq. (3), as is usually done in the treatment of wide gap semiconductors such as Si or Ge. Equation (3) can be analytically solved only in two extreme situations.

(1) For low temperatures $E_F-E_C \gg kT$, the solution is proportional to the activated function $\exp(-E_g/2kT)$, where E_g is the gap energy (Boltzmann approximation). The fit in this temperature range gives $E_g=30$ meV, in excellent agreement with recent photoemission[12] and ellipsometric[27] measurements.

(2) For high temperatures $E_F-E_C \ll kT$, the solution is temperature independent (the semiconductor is totally degenerate) corresponding to the saturation of the linewidth. In FeSi, the saturation is achieved above 250 K.

A numerical integration of Eq. (3) with an appropriate ratio m_n/m_p gives a perfect fit of the experimental data (the triangles in Fig. 3). For temperatures below 150 K, we obtain the fit for a constant value of $m_n/m_p=1$. Consequently, the Fermi level is located in the middle of the gap, as pointed out in Fig. 11. For higher temperatures, the m_n/m_p ratio must be adapted (the new values are attached to the corresponding points in Figs. 10 and 11). As a result, the Fermi level moves toward the valence band and lies within the band at 250 K, corroborating the closing of the gap.[1]

This finding removes one of the apparent contradictions regarding the gap size and the gap closure in the normal semiconductor-band picture. The incompatibility of a gap of 60 meV at low temperatures and the closing of the gap at about 200 K led to the claim that FeSi is a strongly correlated electron system (Ref. 1). However, our present data as well as the gap determination from IR spectroscopy[27] and high-resolution photoemission[12] indicate a smaller gap of only 30 meV. Taking into account the fact that the chemical potential will shift with increasing temperature whenever the effective masses in the valence and conduction band differ allows a self-consistent interpretation of gap energy and gap closure in the framework of simple semiconductor-band theory.

(ii) For metallic CoSi and $Fe_{1-x}Co_xSi$ with $x>0.1$, the temperature dependence of the linewidth shows no sign of additional electron-phonon coupling. The latter would produce a line broadening of the Raman modes already at low temperatures, giving a strong asymmetry of the curve in Fig. 8 around the transition concentration of $x=0.1$. Since this is not the case, one can rule out that electron-phonon interactions play a substantial role for the metallic CoSi and $Fe_{1-x}Co_xSi$ samples with $x>0.1$.

Very recently, Menzel *et al.*[27] performed accurate IR ellipsometry measurements for the whole concentration range of $Fe_{1-x}Co_xSi$. For the semiconductor samples, the spectra were fitted using an asymmetry parameter (Fano line shape), while the phonons of the metallic samples have a typical Lorentz shape. The Fano line shape indicates electron-phonon coupling, in good agreement with our present results.

V. SUMMARY

A complete Raman spectroscopy study of the phonons in $Fe_{1-x}Co_xSi$ for the whole concentration range $0 \leq x \leq 1$ has

been presented. We have identified all the nine Raman modes predicted by the factor group analysis. The frequencies of the Raman lines for FeSi and CoSi were calculated using LDA. There is an encouraging agreement of the energies and succession of the observed and calculated modes. The small matching factor of 1.12 needed to obtain full agreement of the absolute values expresses the too attractive LDA potential.

The linewidths of the Raman modes were analyzed as a function of the Co concentration x and the temperature. We have observed a broadening of the Raman lines with increasing x up to $x=0.5$ followed by a line narrowing between $x=0.5$ and $x=1$. This effect is consistent with the crystallographic disorder induced by the substitution of Co on the Fe sites, with a maximum around the concentration $x=0.5$.

The semiconductor samples show an anomalous strong temperature dependence of the linewidth and saturation above 250 K, in contrast to the metallic samples. The latter have only a small temperature dependence due to phonon-phonon interactions and show no saturation. The electron-phonon coupling is treated within the model introduced by Axe and Shirane.[37] A fit of the temperature dependence of the linewidth of FeSi gives an activation energy of 30 meV, in good agreement with values determined on samples from the same badges by IR[27] and photoemission[12] experiments. This adds arguments against the description of FeSi as a strongly correlated electron system and favors its description as a small-gap semiconductor close to a first-order transition to a ferromagnetic metal.[39]

ACKNOWLEDGMENT

The authors thank T. Lampe from the Institut für Physik der Kondensierten Materie of TU Braunschweig for technical support.

*a.racu@tu-bs.de; http://www.ipkm.tu-bs.de/

[1] Z. Schlesinger, Z. Fisk, Hai-Tao Zhang, M. B. Maple, J. F. DiTusa, and G. Aeppli, Phys. Rev. Lett. **71**, 1748 (1993).
[2] L. Degiorgi, M. B. Hunt, H. R. Ott, M. Dressel, B. J. Feenstra, G. Grner, Z. Fisk, and P. Canfield, Europhys. Lett. **28**, 341 (1994).
[3] A. Damascelli, K. Schulte, D. van der Marel, and A. A. Menovsky, Phys. Rev. B **55**, R4863 (1997).
[4] M. Fäth, J. Aarts, A. A. Menovsky, G. J. Nieuwenhuys, and J. A. Mydosh, Phys. Rev. B **58**, 15483 (1998).
[5] P. Samuely, P. Szabó, M. Mihalik, N. Hudáková, and A. A. Menovsky, Physica B **218**, 185 (1996).
[6] A. Lacerda, H. Zhang, P. C. Canfield, M. F. Hundley, Z. Fisk, J. D. Thompson, C. L. Seaman, M. B. Maple, and G. Aeppli, Physica B **186-188**, 1043 (1993).
[7] K. Breuer, S. Messerli, D. Purdie, M. Garnier, M. Hengsberger, Y. Baer, and M. Mihalik, Phys. Rev. B **56**, R7061 (1997).
[8] P. Nyhus, S. L. Cooper, and Z. Fisk, Phys. Rev. B **51**, R15626 (1995).
[9] T. Jarlborg, Phys. Rev. B **51**, 11106 (1995).
[10] D. Menzel, D. Zur, and J. Schoenes, J. Magn. Magn. Mater. **272-276**, 130 (2004).
[11] D. Menzel, M. Finke, T. Donig, A.-M. Racu, and J. Schoenes, Physica B **378-380**, 718 (2006).
[12] D. Zur, D. Menzel, I. Jursic, J. Schoenes, L. Patthey, M. Neef, K. Doll, and G. Zwicknagl, Phys. Rev. B **75**, 165103 (2007).
[13] H. Poulet, and J. P. Mathieu, *Vibrational Spectra and Symmetry of Crystals* (Gordon and Breach, New York, 1976).
[14] R. Dovesi, V. R. Saunders, C. Roetti, R. Orlando, C. M. Zicovich-Wilson, F. Pascale, B. Civalleri, K. Doll, N. M. Harrison, I. J. Bush, Ph. D'Arco, and M. Llunell, *CRYSTAL 2006 User's Manual* (University of Torino, Torino, 2006).
[15] L. F. Mattheiss and D. R. Hamann, Phys. Rev. B **47**, 13114 (1993).
[16] M. Neef, K. Doll, and G. Zwicknagl, J. Phys.: Condens. Matter **18**, 7437 (2006).
[17] R. Dovesi, F. Freyria Fava, C. Roetti, and V. R. Saunders, Faraday Discuss. **106**, 173 (1997).
[18] K. Doll, V. R. Saunders, and N. M. Harrison, Int. J. Quantum Chem. **82**, 1 (2001).
[19] K. Doll, Comput. Phys. Commun. **137**, 74 (2001).
[20] F. Pascale, C. M. Zicovich-Wilson, F. López-Gejo, B. Civalleri, R. Orlando, and R. Dovesi, J. Comput. Chem. **25**, 888 (2004).
[21] R. Resta, Ferroelectrics **136**, 51 (1992).
[22] R. D. King-Smith and D. Vanderbilt, Phys. Rev. B **47**, 1651 (1993).
[23] R. Resta, Phys. Rev. Lett. **80**, 1800 (1998).
[24] C. M. Zicovich-Wilson, R. Dovesi, and V. R. Saunders, J. Chem. Phys. **115**, 9708 (2001).
[25] M. P. J. Punkkinen, K. Kokko, M. Ropo, I. J. Väyrynen, L. Vitos, B. Johansson, and J. Kollar, Phys. Rev. B **73**, 024426 (2006).
[26] P. Villars and L. D. Calvert, *Pearson's Handbook of Crystallographic Data for Intermetallic Phases* (ASM International, Metals Park, OH, 1985).
[27] D. Menzel *et al.* (unpublished).
[29] J.-Y. Son, K. Okazaki, T. Mizokawa, A. Fujimori, T. Kanomata, and R. Note, Phys. Rev. B **68**, 134447 (2003).
[30] M. K. Chattopadhyay, S. B. Roy, Sujeet Chaudhary, Kanwal Jeet Singh, and A. K. Nigam, Phys. Rev. B **66**, 174421 (2002).
[31] Y. Onose, N. Takeshita, C. Terakura, H. Takagi, and Y. Tokura, Phys. Rev. B **72**, 224431 (2005).
[32] F. P. Mena, J. F. DiTusa, D. van der Marel, G. Aeppli, D. P. Young, C. Presura, A. Damascelli, and J. A. Mydosh, Phys. Rev. B **73**, 085205 (2006).
[33] J. Menendez and M. Cardona, Phys. Rev. B **29**, 2051 (1984).
[34] J. Jimenez, E. Martin, A. Torres, and J. P. Landesman, Phys. Rev. B **58**, 10463 (1998).
[35] J. Bäckström, M. Rübhausen, M. Käll, L. Börjesson, A. P. Litvinchuk, M. Kakihana, M. Osada, and B. Dabrowski, Phys. Rev. B **61**, 7049 (2000).
[36] A.-M. Racu and J. Schoenes, Phys. Rev. Lett. **96**, 017401 (2006).
[37] J. D. Axe and G. Shirane, Phys. Rev. Lett. **30**, 214 (1973).
[38] C. Kittel, *Introduction to Solid State Physics*, 7th ed. (Wiley & Sons, Inc., New York, 1996).
[39] V. I. Anisimov, S. Yu. Ezhov, I. S. Elfimov, I. V. Solovyev, and T. M. Rice, Phys. Rev. Lett. **76**, 1735 (1996).